LA-UR- 97-805

CONF-970531--4

Title:

FINITE ELEMENT PREDICTION OF ELASTIC STRAINS IN BERYLLIUM COMPACT TENSION SPECIMENS

Author(s):

Francisco Guerra, ESA-EA, LANL
Ravi Varma, MST-6, LANL
Mark Bourke, LANSCE/MST-5, LANL
Michael Garcia, ESA-EA, LANL
Ray Green, ESA-EA, LANL
A. Sharif Heger, Department of Chemical and Nuclear Engineering, UNM

Submitted to:

ICONE-5 International Conference on Nuclear Engineering
1997 ASME/SFEN/JSME
May 26 - 30, 1997
Nice, France

MASTER

Los Alamos
NATIONAL LABORATORY

Form No. 836 R5
ST 2629 10/91

DISCLAIMER

Proceedings of ICON 5:
5th International conference on Nuclear Engineering
May 26-30, 1997, Nice, France

ICONE5-2027

FINITE ELEMENT PREDICTION OF ELASTIC STRAINS IN BERYLLIUM COMPACT TENSION SPECIMENS

Francisco Guerra, Mark Bourke, Ravi Varma, Michael D. Garcia, Ray E. L. Green, and A. Sharif Heger*

Los Alamos National Laboratory, Los Alamos, New Mexico 87545, USA

*Department of Chemical and Nuclear Engineering, University of New Mexico, Albuquerque, New Mexico 87000, USA

ABSTRACT

Three-dimensional finite element (FE) calculations using ABAQUS version 5.5.9 were compared to neutron diffraction measurements of a loaded, pre-cracked beryllium compact tension (CT) specimens. The objective was to validate the FE results with the experimental "elastic strain" measurements. Then the FE calculations could be used to study residual stress and other aspects of these problems in the unloaded state and the crack tip stress in the loaded state hard to measure experimentally.

A graded FE mesh was focused on the regions containing high strain gradients, the smallest elements were approximately 0.5 mm x 0.5 mm x 0.4 mm. A standard 20-node brick element model was complemented by a model with 1/4-point elements at the crack tip. Since the neutron diffraction measurements provided a volume average of approximately a cube of edge 3.0 mm, various averaging (or integrating) techniques were used on the FE results. Several integration schemes showed good agreement with the experimental results.

INTRODUCTION

The finite element method is an effective way of approximating a solution to the force and moment equilibrium equations of a solid body (Oden, 1978), (Zienkiewicz, 1977), (Cook, 1981). In general, we seek an approximate solution for the displacements, strains, stresses, and forces in a solid body which has been subjected to some loading history. The existence and convergence of these approximate solutions have also been elegantly demonstrated (Oden, 1978), (Strang *et al.*, 1973). Indeed, convergence studies show that as we increase the level of descretization of the region, the approximate solution approaches an exact solution of the governing differential equations. Similarly, if we use a higher order approximation, i.e. quadratic displacement versus linear, then the rate of convergence also increases. These existence and convergence studies, imply that we can have a degree of confidence in generating an approximate solution for a solid body undergoing loading for which an analytic solution is either not available or practical.

Liebowitz (1989) surveyed numerical methods used in computational fracture mechanics. Finite difference methods, finite element methods, and boundary element methods were the three numerical approaches to the solution of fracture mechanics problems. Strengths and weaknesses were itemized for each method, and finite element methods were found to be better for modeling of three dimensional fracture problems. Atluri *et al.* (1994) discussed recent advances in computational methods in fracture mechanics. Their survey presented (i) boundary integral methods, (ii) analytical solutions for elliptical or circular cracks embedded in isotropic or transversely isotropic solids, (iii) finite-element or boundary-element alternating methods, (iv) domain-integral methods, and (v) methods for generation of weight-functions in 2 and 3-D linear elastic crack problems. These two review papers contain extensive references on the various methods used to study fracture.

In the study of fracture mechanics, finite element solutions have, in some cases, compared well with experimental results. Scammarella *et al.* (1996) used computer-assisted Moiré method to compare experimental and finite element stresses on an aluminum compact tension specimen. Their results agreed well. Another example included work by Narashiman et al. (1989). Erbe *et al.* (1994) who used a grating method to compute strains from the observed deformations on steel compact tension specimens. In that case, two-dimensional plane stress finite element strain contours showed poor correlation with the experimental results; however, a three dimensional model using 10-node tetrahedral elements showed good agreement. Parnas *et al.* (1996) used quadratic, five-noded, plane stress elements in their steel and aluminum compact tension specimens. Their finite elements strains also compared well with their strain gage measurements.

The model and the selection of appropriate material properties we used neutron diffraction (Hutchings *et al.*, 1992) to measure the elastic strain field in a loaded CT specimen. Although neutron diffraction has a limited spatial resolution close to 1 mm, previous examples have effectively measured strain fields resulting from plastic deformation near cracks (Smith *et al.*, 1992). The thrust of this paper concerns the various methods of smoothing the finite element strains for an appropriate comparison with the experimental results. In this case, the finite element results are used to correlate with the neutron diffraction results in the interior of the loaded specimens. Specific advantages of the FE calculations over the experiment are improved resolution in the vicinity of the crack which is important both during and after loading. Details of the neutron diffraction experiments are presented in a companion paper Varma (1997).

BACKGROUND

In this section we will review the key points in the derivation of the finite element method as applied to this class of problems. We follow the derivation in ABAQUS (1996) because of its simplicity. Derivations for more general linear operators can be found in Oden (1978) and Strang *et al.* (1973). Two key concepts in this derivation are equilibrium and virtual work. For an exact solution, both force and moment equilibrium must be maintained over the volume of body at all times. The approximation in the displacement finite element method comes from two sources: (1) relaxing the equilibrium requirement at every point within the volume by requiring only that equilibrium be maintained in an average sense over the volume of the body and (2) that the approximation should represent the displacements over those finite volumes.

Using a Lagrangian viewpoint, if V is the volume occupied by a part of the body in the current configuration, and S is the surface bounding this volume, then we can define the surface traction, **t**, as the force per unit of current area at any point S by

$$\mathbf{t} = \mathbf{n} \bullet \sigma \qquad (1)$$

where σ is the "true" or Cauchy stress matrix at a point on S and **n** is the unit normal to S at the point. Let the body force at any point within the volume of a material under consideration be **f** per unit of current volume. Then the force equilibrium for the volume is

$$\int_S \mathbf{t}\, dS + \int_V \mathbf{f}\, dV = 0 \qquad (2)$$

Using the surface traction's definition (1) in equation (2) and then applying the divergence theorem to (2), we establish the differential equation for translation equilibrium as

$$\left(\frac{\partial}{\partial \mathbf{x}} \right) \Sigma\, \sigma + \mathbf{f} = 0 \qquad (3)$$

where the divergence ($\partial/\partial \mathbf{x}$) is with respect to the current configuration and the equations apply pointwise in the body.

Assuming that no point couples act on the volume, application of the divergence theorem to the moment equilibrium yields the result that the Cauchy stress matrix must be symmetric.

The next step is to cast the solution of the equilibrium equations (3) into a "weak form." This is done by replacing the three equilibrium equations in (3) with a single scalar equation over the entire body. This is achieved by using a weighted residual or Galerkin method in which the scalar equation is obtained by multiplying the pointwise differential equations by an arbitrary, vector-valued "test function", defined, with suitable continuity, over the entire volume, and integrating:

$$\int_V \left[\left(\frac{\partial}{\partial \mathbf{x}} \right) \Sigma\, \sigma + \mathbf{f} \right] \Sigma\, \delta \mathbf{v}\, dV = 0 \qquad (4)$$

Since the test functions $\delta \mathbf{v}$ are arbitrary, equilibrium in any direction can be satisfied by choosing the test function to be nonzero in that direction. For this case of equilibrium with a general stress matrix, this equivalent "weak form" is the virtual work principle. For this case, the test functions are a "virtual" velocity field, $\delta \mathbf{v}$, which must obey any prescribed kinematics constraints and have sufficient continuity.

By applying the chain rule to the term inside the integral of (4), then applying the divergence theorem to that result, we get the virtual work equation

$$\int_V \sigma : \delta D \, dV = \int_S \delta v \sum t \, dS + \int_V \delta v \sum f \, dV \quad (5)$$

where δD, the symmetric part of the velocity gradient in the current configuration, is defined in terms of δv as:

$$\delta D = \frac{1}{2}\left(\frac{\partial \delta v}{\partial x} + \left[\frac{\partial \delta v}{\partial x} \right]^T \right) \quad (6)$$

The weak formulation not only reduces the order of the differential operator, but also loosens the restriction of satisfying the governing differential equations, e.g. equilibrium, by averaging them over an volume which itself can be broken up into a finite number of elements.

Babuska's ((1971) approximation theorem and Ciarlet and Raviart (1972) interpolation theorem established the mathematical fundamentals for the finite element approximations. The basis is representation of the displacements over the finite number of volumes. (For the sake of simplicity have we address only displacements, but other field variables such as temperature, pressure, or stress can be part of the approximations to give mixed or hybrid formulations by Oden (1978, 1976), Zienkiewicz (1977), Strang *et al.* (1973)) The order of the displacement approximation is based on the number of nodes in each element. The element displacement representation can be expressed as,

$$u = N_N \, u^N \quad (7)$$

where N_N are interpolation functions which depend on some material coordinate system, u^N are nodal variables, and the summation convention is adopted for the upper case subscripts and superscript which indicate nodal variables. Introducing these into the virtual field δv, with the assumption that δv be compatible with the kinematics constraints, we then substitute into (5) to establish the finite element approximation to our boundary value problem.

Note that the finite element approximation is for the displacements based on the nodal values. However, in most problems it is the strains and stresses that are of interest, and these quantities involve a differentiation of our approximation. Moan (1974) and Wheeler (1974) showed that for approximations of this kind, the "reduced" integration of the element contributions to (7) are the best points to compute the first derivatives of the displacement approximation and that the boundary are the worst. Hinton (1974) showed numerically that an extrapolation of these Gauss point derivatives to the boundary and averaging with adjacent elements produce good agreement with a least square fit of the Gauss point data onto the nodal points. Guerra (1974, 1977) also made numerical observations that this type of extrapolations and averaging gave very comparable results to Oden's (1972) more rigorous dual space computation of stresses.

FINITE ELEMENT MODEL

Figure 1 shows the dimensions of CT specimens modeled. The neutron diffraction experiments in Varma (1997) "measure" the elastic strains over a cube of edge length approximately 3.0 mm in the interior of the test specimen as shown in the shaded areas of the Figure 1. The beryllium CT specimens were edge approximately 3 mm thick and were machined with 2.0 mm wide notches that terminated in the multiple 45° chevrons. For measurements under a 2135.0 N load, fixture was designed that allowed the bolt holes to be tensioned apart while simultaneously recording the load on a small load cell. The test CT specimen had a fatigue crack of approximately 6.35 mm.

Figure 2 shows the finite element mesh used with ABAQUS 5.5.9 (ABAQUS, 1996). One quarter of the specimen was modeled with 7178 quadratic 20-node brick elements with reduced integration. In the vicinity of crack tip (EF), the minimum element sizes was 0.5 by 0.5 by 0.42 mm because of the expected high strain gradients, where as at the outer edge (BD) they were 1.97 by 0.5 by 0.42. In addition, mid-side nodes on element edges adjacent to the crack tip (EF) were moved to the quarter point. Henshell et al. (1975) and Koers (1989) showed in numerical experiments that midside nodes at the quarter-point for quadratic (8-node quadrilaterals in 2-dimensions and 20-node bricks in 3-dimensions) elements gave favorable results in crack tip studies and were more economical to use than the more accurate hybrid crack elements. Symmetry conditions were imposed on the 2-plane=0 (ACGH) and on the 3-plane=0 (EFCD), and the crack surface (AEFB) was left free. Since the bolt holes were not of interest and distant from the crack region, the hole geometry was not modeled and half the tensile load, 1067.5 N, was equally distributed along the eleven nodes through the model thickness at point K. One of these nodes was also constrained in the 1-direction.

Table I shows the beryllium material properties from Brush Wellman (1983) used. A simple bi-linear elastic-plastic model for ABAQUS. (A more sophisticated piece-wise linear elastic-plastic stress-strain definition could have been used ABAQUS if such material properties for this particular beryllium sample were available.)

Table I. Material properties used for beryllium in the finite element calculations.

Elastic modulus	303690 MPa
Poisson ratio	0.1
.2% yield stress	230 MPa
Ultimate stress	450 MPa
% elongation	0.2

RESULTS

Figure 3 is an enlarged view of the region where the strain measurements were compared. This enlargement of the mesh shows the paths (rows) of elements and nodal points over which the finite element and experimental comparisons were made in the subsequent figures. Since ABAQUS strains were being computed at the best possible points for 20-node brick elements used, i.e. 2 by 2 by 2 Gauss points, our study of the results concentrated on a suitable averaging scheme for comparison with the experiment. Notably the quarter point elements yielded at maximum strain 35% higher than the standard elements, only the quarter point results are presented.. ABAQUS Post was used to extract the elastic strain component in the tensile direction (EE33, perpendicular to the crack plane ABDC) from the total strains. We also limited our focus to the comparison of nodal averages and element averages with the experimental results.

Figure 4 compares the averaged nodal values along path A (EE33PA) and C (EE33PC) with the experimental values (4PKA) at full load. In this and subsequent comparisons, the "absolute distance" is measured from point B ,on surface (ABGH) at the back of the specimen, to point A, at the tip of the chevron, in Figure 2. In Figure 3, nodal path A is shown from the tip of the chevron to the back, and nodal path C is the row of nodes above it. The elements adjacent to these row of nodes were also part of the numerical studies. The maximum experimental elastic strain from 4PKA was 5.20E-04. Figure 5 compares the ABAQUS nodal point running averages of EE33PA for one element (3 nodal points, PAAV3P) and three elements (7 nodal points, PAAV7P) on path A with the experimental results at full load. The choice of three elements was made to correspond with 3 mm cube in the test sample region. The running averages seem to show reasonable agreement with the experimental results and were very practical to use.

A simple FORTRAN program was written to average the eight integration point values for a given element. Figure 6 compares the experimental results with the element averaged values along three rows of elements on the midsurface: (1) PA_AV_EL, the elements along path A, (2) PC_AV_EL, the elements along path C, and (3) PD_AV_EL, the row of elements above (2). These results were also at full load. (The element values are plotted at respective element's mid-side node, starting from point C to A in Figure 2.) The values for the elements two elements in the 2-direction were similar to PD_AV_EL. Averaging PA_AV_EL, PC_AV_EL, and PD_AV_EL. Figure 7 compares the running average of three elements (3 points) of P_A_AVE with the experimental results. Figures 6 and 7 show that the running averages show the good agreement with the experimental results. Because most of the higher gradients occur near the crack tip, the data smoothing seemed to primarily affect the magnitude of the elastic strains there. Table II summarizes the maximum elastic strains (EE33) from the various data smoothing for analyses standard and quarter-point elements in the vicinity of the crack tip.

Finally, Figure 8 plots the nodal point elastic strains (EE33PAA) and the running average over seven nodal points along path A for the unloaded CT specimen.

Table II. Maximum values of elastic strain for the various types of data smoothing.

Experiment 4PKA	5.20E-04	
Case	Standard Element	1/4 Pt. Element
EE33PA	8.89E-04	13.7E-04
EE33PC	5.90E-04	6.44E-04
PAAV3P	6.92E-04	9.61E-04
PAAV7P	5.06E-04	6.23E-04
PA_AV_EL	4.30E-04	8.92E-04
PC_AV_EL	5.51E-04	5.54E-04
PD_AV_EL	4.28E-04	4.34E-04

SUMMARY AND CONCLUSIONS

The finite element method has been shown in the literature to provide a valid approximation for a well posed boundary value problem. For the simple geometry of the CT specimen considered here, our "coarse" finite element mesh calculations compare reasonably with yet another experimental method, neutron diffraction. For beryllium, this is a unique approach since comparable x-ray diffraction measurements have be very hard to obtain. Because the neutron diffraction measurements are taken over finite volumes, various methods for smoothing the finite element results were shown to compare well with the experimental results. A simple running average of nodal values over several elements yielded a comparable results with little effort.

Studies of the crack tip region in more detail using meshes with finer densities at the region are possible. Another more sophisticated local mesh refinement at the crack tip can be achieved with element necklacing. With the availability of various types of contact between surfaces, regions with differing mesh densities can be easily coupled. Another practical method for limited computer resources, is the interpolation of a solution over a selected region from a coarse mesh, such as the one considered here, onto a much finer descretization of that region.

Experimental results have shown that beryllium is not an isotropic or very ductile material. In our analysis we simplified the problem by assuming an isotropic material. In addition, we assumed a von Mises yield surface and a ductile metal plasticity formulation for our problem. Material data such as Young's

modulus, Poisson's ratio, and true plastic stress-strain data generated from tests on the actual material have been shown to greatly improve the finite element results. And more sophisticated material models are available in ABAQUS and the literature which could also improve the finite element simulations.

ACKNOWLEDGMENTS

This work was supported by the Department of Energy under contract W-7405-ENG-36 through the Enhanced Surveillance Program and the Science Based Stockpile Stewardship Program.

REFERENCES

Oden, J. T, E. B. Becker, and G. Carey, 1981, *Introduction to the Finite Element Method,* Prentice-Hall, Englewood Cliffs, New Jersey, 1981.

Zienkiewicz, O. C., 1977, *The Finite Element Method in Engineering*, 3nd Ed., McGraw Hill, London.

Cook, R. D., 1981, *Concepts and Applications of Finite Element Analysis,* Wiley & Sons, New York.

Strang, G., and G. Fix, 1973, *An Analysis of the Finite Element Method,* Prentice Hall, Englewood, New Jersey.

Liebowitz, H., 1989, "Computational Fracture Mechanics", *7th International Conference on Fracture Mechanics.*, Houston, Texas, 1887-1921.

Atluri, S. N. and T. Nishioka, 1994, "On Some Recent Advances in Computational Mechanics of Fracture", *Fracture Mechanics: 26th Volume, ASTM STP 1256*, Idaho Falls, Idaho, 1923-1967.

Sciammarella, C. A. , and O. Combel, 1996, "An Elasto-plastic Analysis of the Crack Tip Field in a Compact Tension Specimen", *Engineering Fracture Mechanics*, Vol. 55, No. 2, 209-222.

Narasimhan, R, A. J. Rosakis, and B. Maran, 1989, *A Three Dimensional Numerical Investigation of Fracture Initiation by Ductile Failure Mechanisms in A4340 Steel*, SM Report 89-5, California Institute of Technology, Pasadena, California.

Erbe, M., K Galanulis, R. Ritter and E. Steck, 1994, "Theoretical and Experimental Investigations of Fracture by Finite Element and Grating Methods", *Engineering Fracture Mechanics,* Vol. 48, No., 103-118.

Parnas, L. and O. G. Blair, 1996, "Strain Gage Methods for Measurement of Opening Mode Stress Intensity Factor, *Engineering Fracture Mechanics*, Vol. 55, No. 3, 485-492.

Smith, D. J., M. A. M. Bourke, A. P. Hodgson, G. A. Webster, P. J. Webster, 1992, "Interpretation of Residual Stress Distributions in Previously Loaded Cracked Beams, *Journal of Strain Analysis*, Vol. 27, No. 2.

Varma, R., M. Bourke, M. D. Garcia, R. E. L. Green, and F. Guerra, 1997, "Experimental and Numerical Determination of Strains in Beryllium Compact Tension Specimens, *Proceedings of 5th International Conference on Nuclear Engineering,*, Nice, France.

ABAQUS Theory Manual, 1996, Hibbitt, Carlson, and Sorensen, Inc., Providence, Rhode Island.

Babuska, I., 1971, "Error-bounds for Finite Element Methods", *Numerical Methods*, Vol. 16, 322-333.

Ciarlet, P. G., and R. A. Raviart, 1972, "Interpolation Theory Over Curved Finite Elements with Applications to Finite Element Methods", *Computational Methods in Applied Mechanical Engineering*, Vol. 1, 217-249.

Oden, J. T., and J. N. Reddy, 1976, *Variational Methods in Theoretical Mechanics*, Springer-Verlag, New York.

Moan, T., 1974, "Orthogonal Polynomials and 'Best' Numerical Integration Formulas on a Triangle, *ZAMMA*, 54, 501-508.

Wheeler, M. F., 1974, "A Galerkin Procedure for Estimating the Flux for Two-point Boundary Value Problems", *SIAM Numerical Analysis*, Vol. 11, No. 4.

Hinton, E., and J. S. Campbell, 1974, "Local and Global Smoothing of Discontinuous Finite Element Functions Using a Least Squares Method", *International Journal on Numerical Methods in Engineering*, Vol. 8, 461-480.

Guerra, F. M., 1974, *An Automated Scheme for the Coarse-to-Fine Mesh Method*, Masters thesis, The University of Texas at Austin.

Guerra, F. M., 1977, *Finite Element Analysis for the Adaptive Method of Rezoning,* PhD Dessertation, The University of Texas at Austin.

Oden, J. T., 1972, *Finite Elements of Nonlinear Continua*, McGraw-Hill, New York.

Desiging with Beryllium, 1983, Brush Wellman, Inc., Cleveland, Ohio.

Hutchings, M. T., and Krawitz, A. D., ed., 1992, *Measurement of Residual and Applied Stress Using Neutron Deffraction*, NATO ASI Series 216E, Kluwer Academic Publishers, Dordrecht / Boston / London, 93-112.

Henshell, R. D., and K. G. Shaw, 1975, "Crack Tip Finite Elements Are Unnecessary", *International Journal for Numerical Methods in Engineering*, Vol. 9, 495-507.

Koers, R. W. J., 1989, "Use of Modified Standard 20-node isoparametric Brick Elements for Representing Stress/Strain Fields at a Crack Tip for Elastic and perfectly Plastic materials", *International Journal of Fracture*, Vol. 40, 79-110.

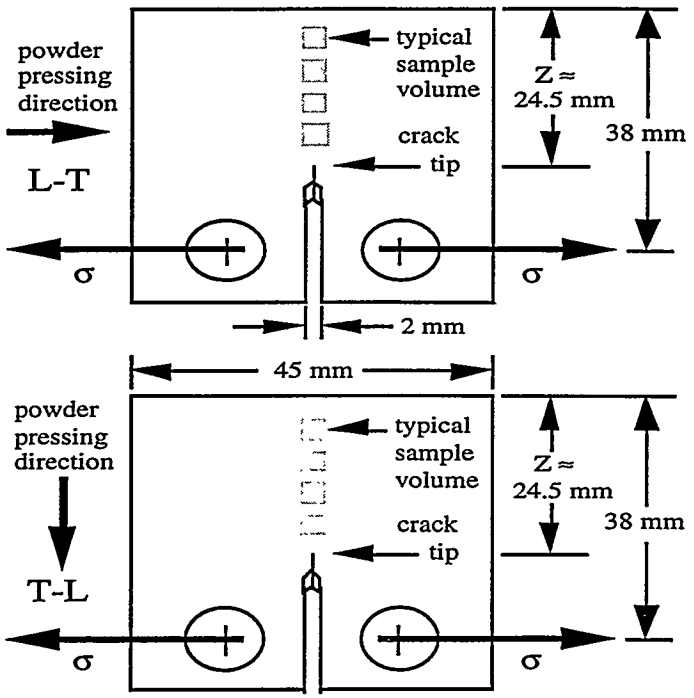

Figure 1. Relative texture designations (L-T and T-L) for the beryllium CT specimens with respect to the material powder pressing direction.

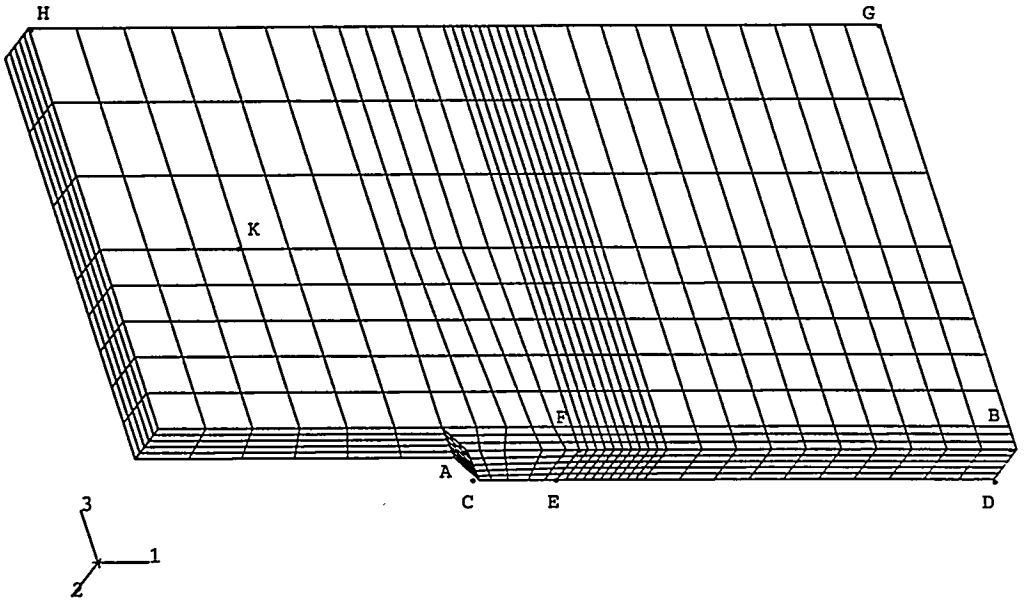

Figure 2. Finite element mesh used to model one quarter of the specimen.

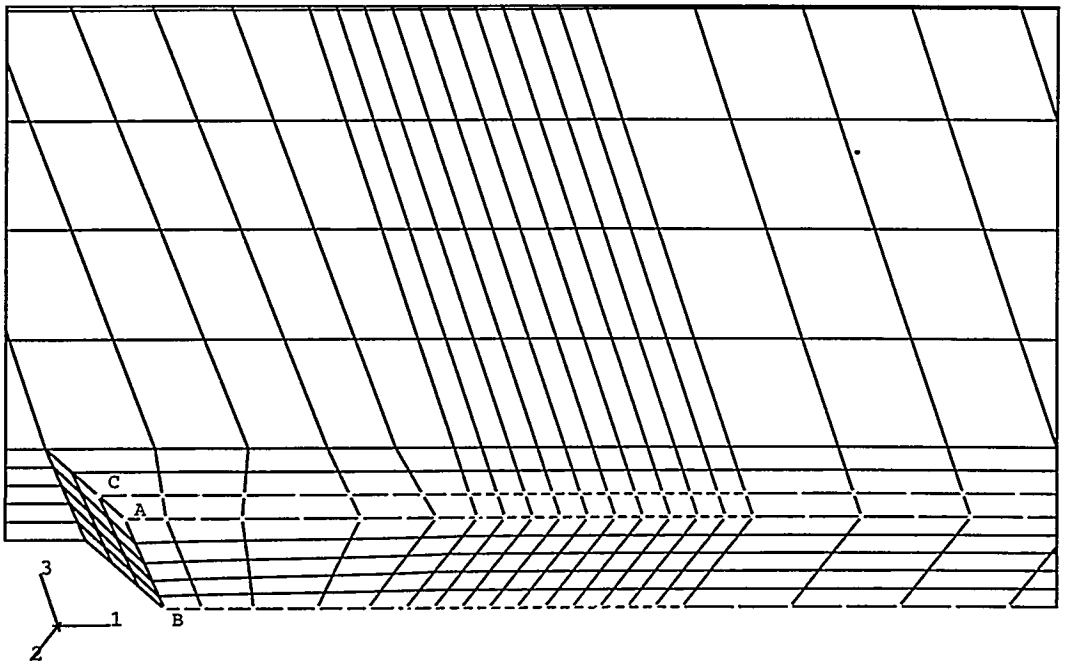

Figure 3. Nodal and element paths used for smoothing of the finite element results.

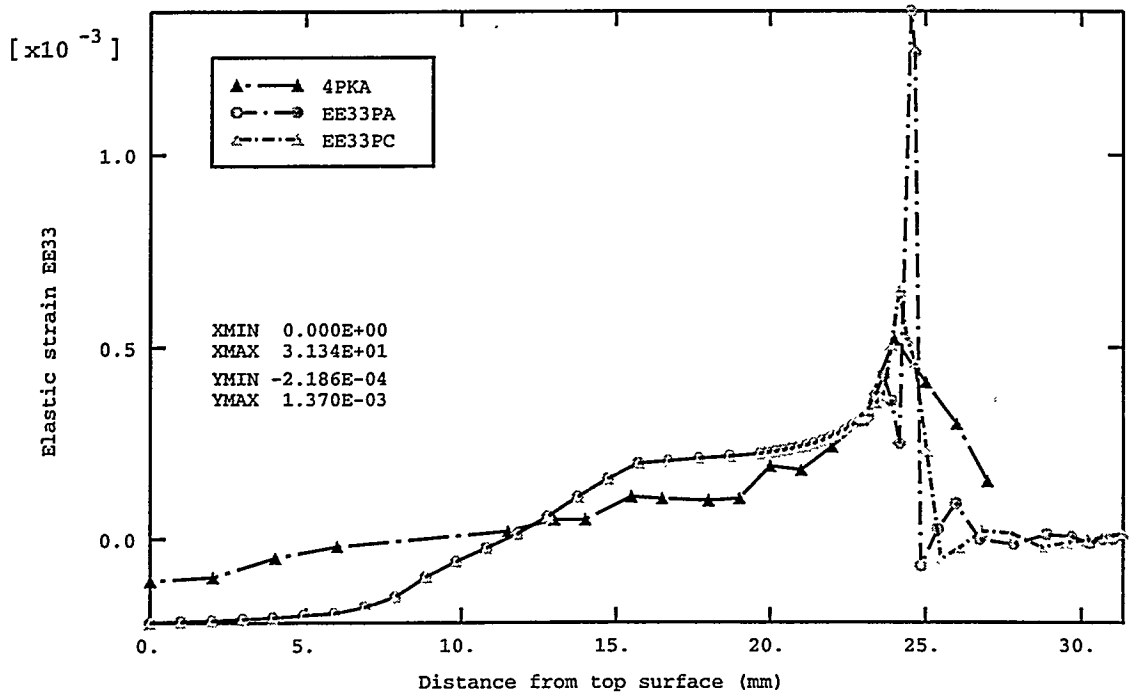

Figure 4. Finite element nodal averages along path A (EE33PA) and path C (EE33PC) comparison with experimental results (4PKA).

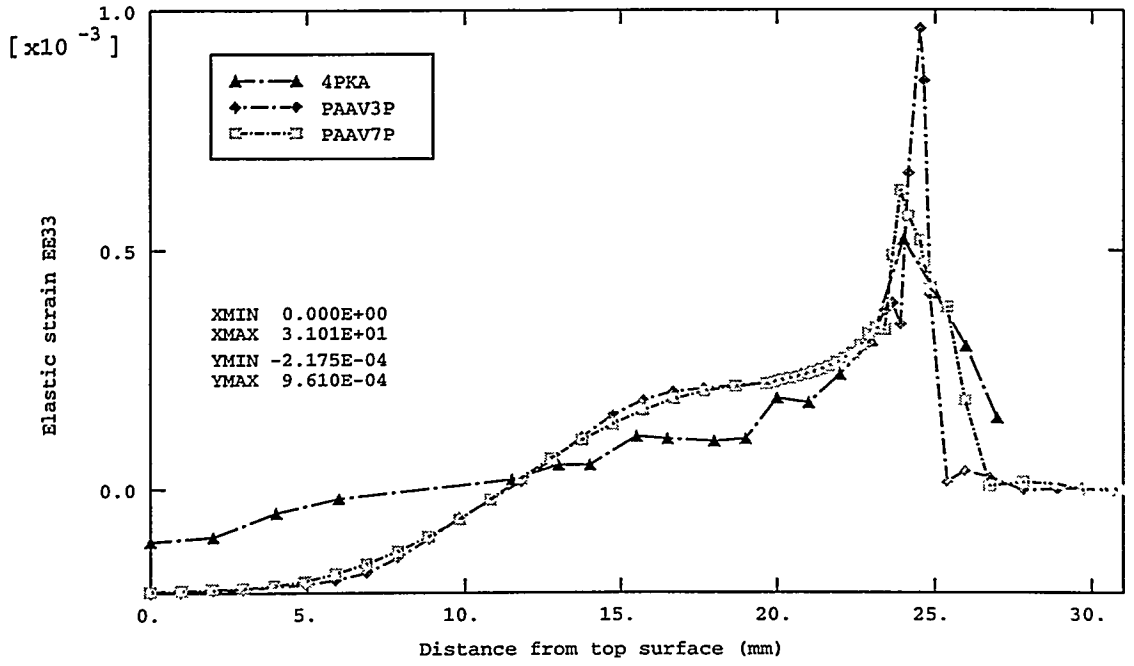

Figure 5. Comparison of path A running averages for one element (PAAV3P) and three elements (AAV7P) with experimental results (4PKA).

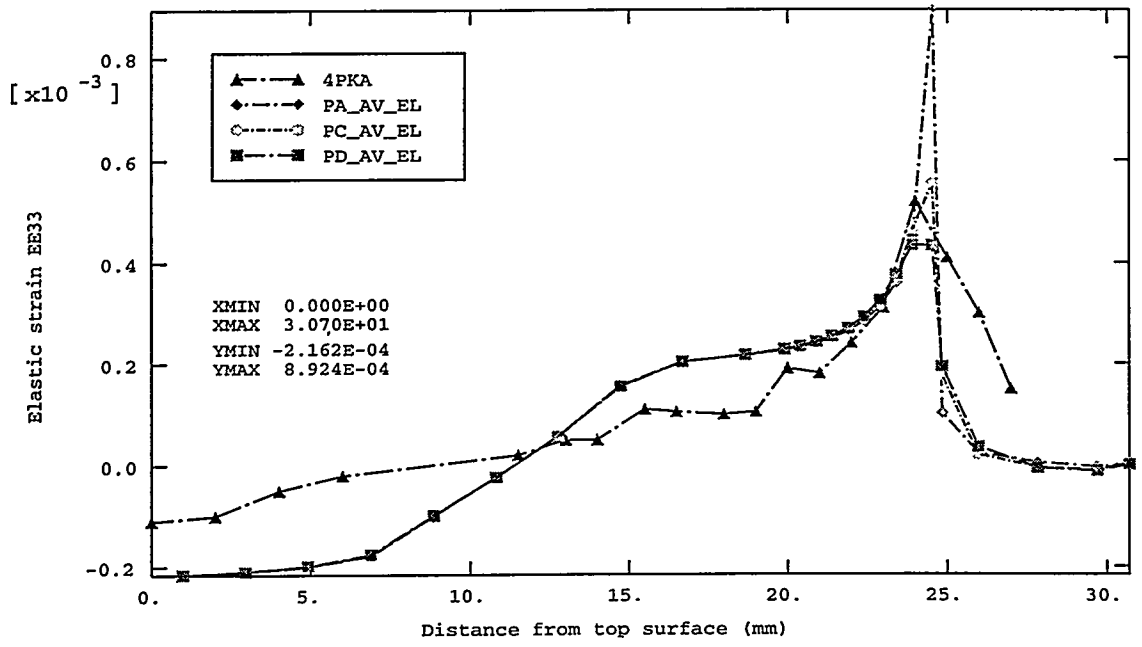

Figure 6. Comparison of averaged element integration point values along three rows of elements on the mid-surface and experimental results.

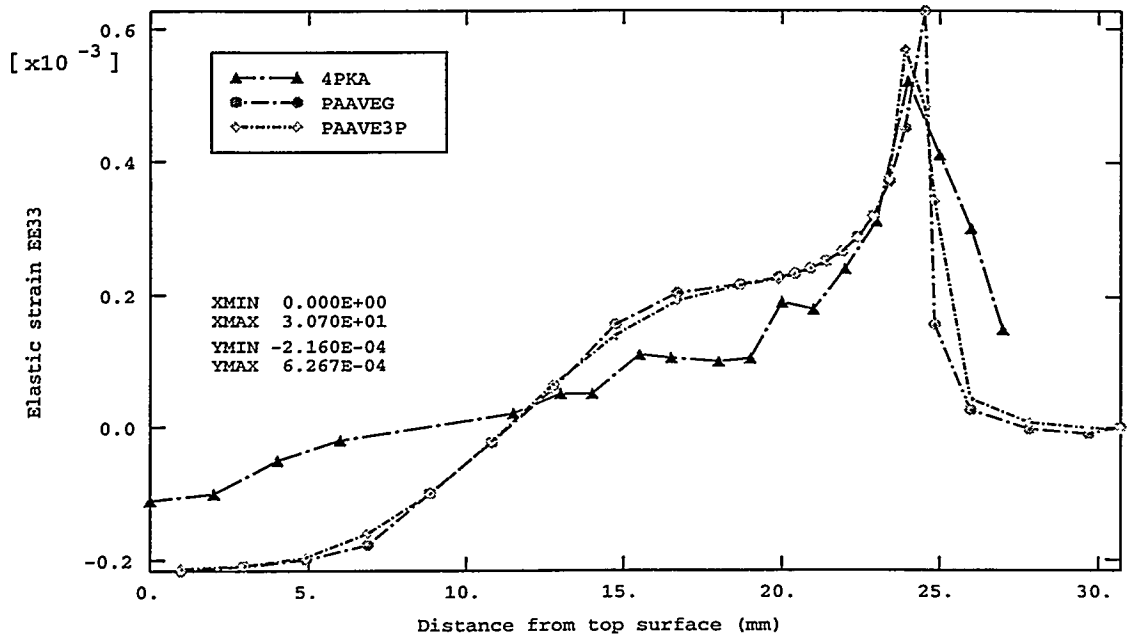

Figure 7. Comparison of running averages of the element values with experimental results.

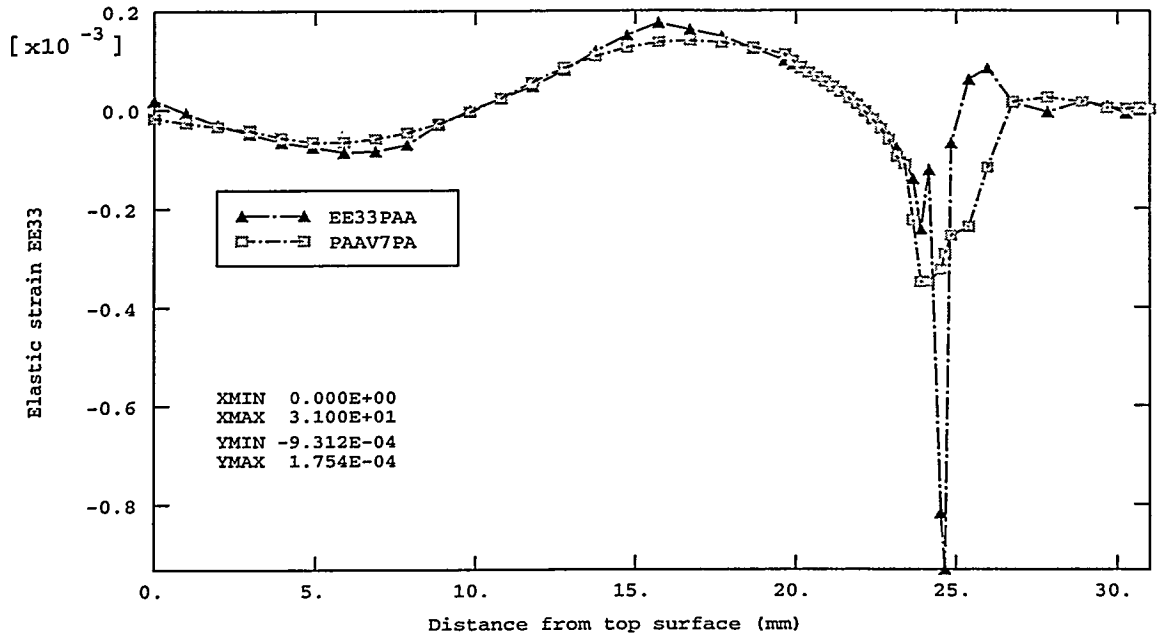

Figure 8. Path A residual elastic strains (EE33PA) and the three element running average (PAAV7PA) for the unloaded specimen